

Aspects of Spacecraft Charging in Sunlight

Shu T. Lai, *Fellow, IEEE*, and Maurice F. Tautz, *Member, IEEE*

Abstract—This paper is an overview of spacecraft charging in sunlight. The daylight photoelectron flux emitted from spacecraft surfaces normally exceeds the ambient electron flux. As a result, charging of spacecraft surfaces to positive voltage is expected to occur in sunlight. Indeed, spacecraft are often observed to charge to low positive voltages in sunlight. However, spacecraft can charge to high-level (kiloelectronvolts) negative voltages in sunlight. Why do spacecraft charge negatively in sunlight? One chief reason concerns differential charging between the sunlit and dark sides. For a satellite with dielectric surfaces, an electric field builds up on the shaded surfaces and then wraps around to the sunlit side to form a potential barrier that suppresses the photoemission. A monopole–dipole (for zero spin) or monopole–quadrupole model (for fast spin) describes the differential charging potential distribution due to blocked photoelectrons. It is shown that these cases are similar to a more general multipole potential field in that the surface node potentials satisfy an approximate linear relation. These cases are all driven by the shade side charging so that the onset for charging is approximately the same in sunlight or eclipse if conduction currents through the spacecraft can be neglected. If conduction currents are important, potential barriers can develop on the dark side, leading to suppression of the secondary emission currents and modification of charging onset. The results were briefly compared with observations. Another important reason for negative charging concerns reflectance. Highly reflective mirrors generate substantially reduced photoemission so that current balance can be achieved without barrier formation. The onset for charging in this case depends strongly on the reflectivity. The critical temperature for charging of surface materials under space substorm conditions with different ratios of photoemission current to electron ambient current, corresponding to varying satellite surface reflectivity values, was calculated. Numerical results, which show that with substantially reduced photoemission, highly reflective surfaces charge in sunlight with the critical temperature for onset decreasing with increasing reflectivity, are presented.

Index Terms—Monopole–dipole, monopole–quadrupole, photoemission, reflectance, spacecraft charging, sunlight charging.

NOMENCLATURE

A	Dipole term normalized to K .
A_{nm}, B_{nm}	Coefficients of potential expansion.
B	Potential barrier height.
dA	Element of surface area.
I_{ph}, J_{ph}	Photoelectron current, photoelectron flux.
I_e, J_e	Ambient electron current, ambient electron flux.
J_o	Photon flux.

K	Monopole potential (normalized by distance).
P	Ratio of I_{ph} and I_e .
P_n^m	Associated Legendre function with indices n and m .
Q	Quadrupole term normalized to K .
q_e, q_i	Electron charge, ion charge.
R, R_o	Surface reflectance, surface reflectance for normal photon incidence.
r	Distance from the satellite center.
r_s	Location of barrier measured from the satellite center.
s	Ratio of Sun intensity at the spacecraft over the 1 AU value.
T_e, T_i	Ambient electron temperature, ambient ion temperature.
T^*	Critical temperature for the onset of spacecraft potential.
V	Potential.
V_P, V_M	Average pole potential, average bellyband potential.
V_{Sun}, V_{shade}	Potential of the sunlit surface, potential of the shade surface.
x	Cosine of polar angle in the Legendre polynomial.
X, Y, Z	Rectangular coordinates in the space frame.
Y	Photoelectron yield per absorbed photon.
Y_n	Photoelectron yield per absorbed photon for normal photon incidence.
δ	Secondary electron emission coefficient.
η	Backscattered electron emission coefficient.
α	Sun angle with respect to the surface normal.
θ	Polar angle with respect to the spin axis.
χ	Ratio of the potentials on the sunlit and shade surfaces.
ω	Photon frequency.

I. INTRODUCTION

SATELLITE charging in space plasmas is due to the imbalance of surface currents. One has to take into account the incident space plasma currents and the secondary and backscatter currents resulting from interactions with the satellite surface materials. If these currents are unbalanced, the spacecraft will charge, which enhances some currents and reduces others, until balance is restored. At the geosynchronous environment, charging in eclipse is often toward high negative voltage because the ambient high-energy (kiloelectronvolts) electron flux exceeds that of the positive ions by two orders of magnitude [1], [2] and the secondary plus backscatter electron yields are well below unity at high energies. In response, the spacecraft goes to a negative potential, repelling some of the incoming

Manuscript received November 22, 2005; revised June 30, 2006. The work of M. F. Tautz was supported by USAF Contract F19628-00-C-0089.

S. T. Lai is with the Space Weather Center of Excellence, Space Vehicles Directorate, Air Force Research Laboratory, Hanscom Air Force Base, Bedford, MA 01731-3010 USA (e-mail: Shu.Lai@hanscom.af.mil).

M. F. Tautz is with the Atmospheric and Environmental Research (AER)/Radex, Inc., Lexington, MA 02421 USA.

Color versions of Figs. 2, 3, and 5 are available at <http://ieeexplore.ieee.org>. Digital Object Identifier 10.1109/TPS.2006.883362

electrons and attracting ions. At equilibrium, all of the currents achieve balance [3], [4].

In sunlight, one has to add the effect of the photoemission current. Laboratory measurements show that the photoelectron flux emitted from typical surface materials illuminated by artificial sunlight greatly exceeds that of the ambient electrons under normal conditions at geosynchronous altitudes [5]–[8]. If the outgoing electron flux exceeds that of the incoming one, charging should be toward positive voltage. Indeed, surface charging to a few positive volts is often observed in sunlight at geosynchronous altitudes [9]–[11]. Positive potentials up to tens of volts have also been reported for spacecraft in the magnetotail or nearer the Sun where far ultraviolet (UV) lines become more intense [12].

Surprisingly, high-level negative voltage (negative kilovolts) charging of spacecraft surfaces is sometimes observed in daylight [13]–[15]. How can high-level negative potential charging occur on spacecraft surfaces in spite of the dominant photoelectron current? An answer is provided by differential charging and surface reflectance.

Potential wells and barriers can form as a result of differential charging between surfaces [16]–[23]. Since photoelectrons are of low energy, they are easily blocked by potential barriers and trapped in potential wells. When the escaping photoelectrons are suppressed, current balance can be achieved, and charging to high negative values can occur. The simplest type of differential charging based on blocked photoelectrons is in the monopole–dipole form [14], [15], [24]–[26]. With a fast spinning satellite, a monopole–quadrupole form is possible [27]. Multipole models are discussed in Sections II–IV. Surface reflectance will reduce the photoelectron current emitted. High-reflectance surfaces have relatively low photoemission and can allow current balance to be reached without barrier formation. Surfaces with high reflectivity can, therefore, charge to negative potentials in hot plasmas despite sunlight [28]. The effects of reflectivity are discussed in Sections V and VI. Conclusions are given in Section VII.

II. MULTIPOLE MODELS

The monopole–dipole potential distribution [26], [29] of a sphere is given by

$$V(\theta, r) = K \left(\frac{1}{r} - \frac{A \cos \theta}{r^2} \right) \quad (1)$$

where V is the potential at a point outside the sphere with a distance r from the sphere center, θ is the polar angle with $\theta = 0^\circ$ facing the Sun, K is the monopole strength, and A is the dipole strength normalized by K . When high-level charging occurs, K equals several (negative) kilovolt meters typically. The potential barrier, which is located toward the Sun at r_S , is determined by

$$\left[\frac{dV(0^\circ, r)}{dr} \right]_{r=r_S} = 0 \quad (2)$$

which gives $r_S = 2A$ from (1). The barrier is located outside the spacecraft ($r > 1$), which sets a threshold $A = 1/2$. The

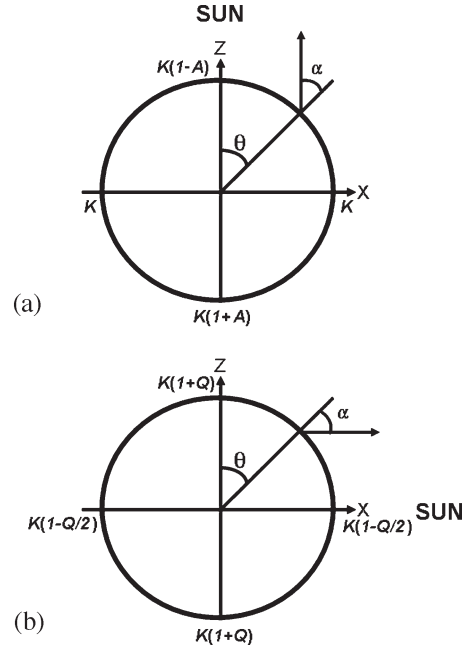


Fig. 1. (a) Monopole–dipole configuration. (b) Monopole–quadrupole configuration.

barrier height B is given by

$$\frac{B}{K} = \frac{V(0^\circ, r_S) - V(0^\circ, 1)}{K} = \frac{(2A - 1)^2}{4A}. \quad (3)$$

A barrier height of even a few volts (negative volts) is sufficient to block photoemission because photoelectrons emitted from geosynchronous satellites have low energies. The characteristic temperature is 1–2 eV [5]–[7], [11]. For high-level charging, the ratio B/K is, therefore, nearly zero, which implies that $A \approx 1/2$ in (3). As a result, (1) yields the ratio χ of the sunlit surface potential to that of the shaded surface

$$\chi = \frac{V(0^\circ, 1)}{V(180^\circ, 1)} = \frac{1 - A}{1 + A} \approx \frac{1}{3}. \quad (4)$$

In Fig. 1(a), we show the monopole–dipole configuration in an (X, Z) Cartesian frame. The Sun’s direction is toward $+Z$. The polar angle and the angle of incidence for photoemission are indicated. The photosheath barrier forms outside of the surface at $+Z$. The surface potentials at the coordinate nodes $+Z$, $-Z$, $+X$, and $-X$ are given in terms of the model parameters K and A . By symmetry, the potentials at $+Y$ and $-Y$ (not shown) are equal to K .

The equilibrium value of A depends on current balance to the spacecraft, where the net current depends on the incident ambient fluxes (which can be parameterized by the density and temperature of each particle species) integrated with the surface material properties. In the theory of critical temperature, the ambient electron temperature T_e is an important space plasma parameter controlling the onset of spacecraft charging. Characterizing the ambient space plasma by T_e , we have found that, statistically, the ratio χ of the satellite potentials with and without sunlight is about 1/3 on the Los Alamos National Laboratory (LANL) geosynchronous satellites no matter which

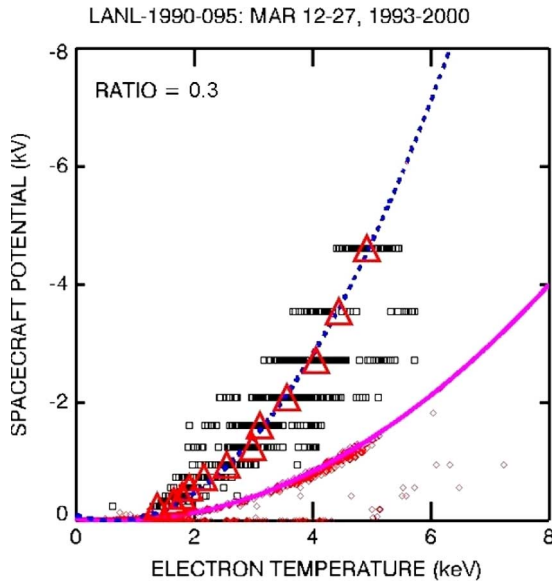


Fig. 2. (Upper branch) charging in eclipse and (lower) in sunlight. The data are quantized because of flux channels. The centroid of the temperature at every quantized level is shown as triangle. The ratio of the two branches is about 0.3.

satellite, year, or month [14], [15], [30]. A sample data plot is shown in Fig. 2.

If the satellite is rotating fast with respect to the surface capacitance charging time, a quadrupole component appears in the potential distribution. For arbitrary sunlight direction, the potential distribution, including any potential barriers, would be symmetrical not about the sunlight direction but, instead, about the spin axis. If the Sun's angle θ with respect to the spin axis is equal to 90° , a dominant monopole–quadrupole potential distribution occurs [27]. The potential then has the following form:

$$V(\theta, r) = K \left[\frac{1}{r} + \frac{Q}{2r^3} (3 \cos^2 \theta - 1) \right]. \quad (5)$$

We can again find a potential barrier using (2). Solving for the radius r_S of the barrier gives $r_S = (3Q/2)^{1/2}$ and a corresponding threshold of $Q = 2/3$. The barrier has a more complicated form than in (3) and is given by

$$\frac{B}{K} = \frac{V(90^\circ, r_S) - V(90^\circ, 1)}{K} = \left(\frac{2}{3}\right)^{3/2} Q^{-1/2} + \frac{Q}{2} - 1. \quad (6)$$

Like (3), this expression is zero at threshold and increases monotonically with Q above the threshold. Here, again, we can obtain a Sun/shade potential ratio near the threshold as

$$\chi = \frac{V(90^\circ, 1)}{V(180^\circ, 1)} = \frac{1 - Q/2}{1 + Q} \approx \frac{2}{5}. \quad (7)$$

In this case, the spin equator (bellyband) is sunlit, and the shaded surfaces occur at the spin poles. Fig. 1(b) shows schematically the potentials at the sphere surface for the monopole–quadrupole configuration. The sphere is spinning around the Z axis, and the Sun's direction is at $\theta = 90^\circ$. The

surface node potentials are given at $+Z$, $-Z$, $+X$, and $-X$ as functions of K and Q . The model potentials at $+Y$ and $-Y$ (not shown) are equal to $K(1 - Q/2)$.

If the Sun's direction θ is situated between 0° and 90° , we find an approximate Sun/shade potential ratio $\chi(A, \theta)$ that goes between the two aforementioned cases [27]. Although there are differences in details, the basic mechanism is the same: The shaded side charges, and the fields wrap around to form a potential barrier that acts to suppress the photoemission.

III. RELATION BETWEEN SATELLITE SURFACE NODE POTENTIALS

We consider the charging in sunlight of a satellite in a low-density plasma. By the standard method of separation of variables, Laplace's equation can be solved in spherical coordinates (r, θ, ϕ) in the following form:

$$V = \frac{K}{r} \left[1 + \sum_{n=1}^{\infty} \frac{1}{r^n} \sum_{m=0}^n P_n^m(x) \times (A_{nm} \cos(m\phi) + B_{nm} \sin(m\phi)) \right]. \quad (8)$$

Here, K/r is the monopole potential, and $P_n^m(x)$ are the associated Legendre functions, with $x = \cos \theta$. The sum over n goes from 1 to ∞ and encompasses the multipole contributions. The sum over m goes from 0 to n and allows for possible azimuthal dependence. The constants K , A_{nm} , and B_{nm} are set by the external conditions. The potentials in (8) vanish at $r = \infty$; otherwise, the solution is quite general.

We consider the surface potentials at the six coordinate nodes, i.e., $+X$, $-X$, $+Y$, $-Y$, $+Z$, and $-Z$, in the space frame of reference. If we take the sum of these node potentials, we obtain

$$V(+X) + V(-X) + V(+Y) + V(-Y) + V(+Z) + V(-Z) = 6K. \quad (9)$$

The calculation of this result is given in the Appendix. It depends only on the properties of the Legendre functions. There are no assumptions about the coefficients K , A_{nm} , and B_{nm} or the symmetry of the potential distribution. It is valid for a summation in (8) from $n = 1$ up to $n = 3$ only. Although the result has been proven only for this limited range, the lower order multipoles typically represent the bulk of the charging distribution.

Consider the Besse–Rubin limit at zero spin [26]. Let the sunlight be incident from $Z = +\infty$. The bellyband potentials are known to be equal to K , and the shade side potential $V(-Z) = K(1 + A)$ [see Fig. 1(a)]. Solving the linear equation (9) for the Sun/shade potential ratio, we get

$$\frac{V(+Z)}{V(-Z)} = \frac{2K}{V(-Z)} - 1 = \frac{1 - A}{1 + A} \quad (10)$$

which is in agreement with (4). Now, put the Sun's direction toward $+X$. This is a Besse–Rubin system with the Sun's

direction rotated from $+Z$ to $+X$. The transverse rim potentials become $V(Y) = V(-Y) = V(Z) = V(-Z) = K$, and the potential on the dark side goes to $V(-X) = K(1 + A)$. The linear equation (9) again leads to (10), but with Z replaced by X , and the same Sun/shade ratio is obtained. In this configuration, there is no azimuthal symmetry around the Z -axis. This example illustrates the generality of the approximate relation (9). Whatever the Sun's direction, the surface node potentials adjust so that they sum to $6K$.

Let us define the average pole potential as

$$V_P = \frac{1}{2}(V(+Z) + V(-Z)) \tag{11}$$

and the average middle (bellyband) potential as

$$V_M = \frac{1}{4}(V(+X) + V(-X) + V(+Y) + V(-Y)). \tag{12}$$

Then, we can write (9) as

$$V_P = 3K - 2V_M. \tag{13}$$

This simple linear relation between the average pole and average bellyband potentials holds up to third order in the multipole expansion for any satellite that satisfies Laplace's equation in spherical coordinates.

We now assume that the satellite is spinning fast around the Z -axis and that the Sun's direction lies somewhere in the bellyband plane. The value of $V_M = K(1 - Q/2)$ [27] at the fast spin limit [see Fig. 1(b)]. For a spinning satellite with the bellyband sunlit, the Sun/shade ratio from (13) goes into

$$\frac{V_M}{V_P} = \frac{V_M}{3K - 2V_M} = \frac{1 - Q/2}{1 + Q} \tag{14}$$

which is in agreement with (7).

The actual coefficients K , A_{nm} , and B_{nm} and the potentials V_M and V_P could be complicated functions of the plasma environment, the satellite current collection characteristics, the surface material properties, and the photoemission sheath structure, but the simple linear relation (9) should always be approximately valid.

IV. ONSET OF SPACECRAFT CHARGING IN SUNLIGHT

In the Maxwellian space plasma model, the onset of spacecraft charging in eclipse occurs at a critical temperature T^* [31]–[35]. If the plasma electron temperature T is below T^* , no charging occurs. Above T^* , the charging voltage increases as the temperature T increases. This property has been observed on the LANL satellites [2]. In sunlight, the abundant outgoing photoelectrons greatly affect the current balance. Naturally, the following question arises: Does a critical temperature T^* exist in sunlight?

At the spin limits, the multipole models indicate that the sunlit side potentials are scaled by a factor χ from the shaded potentials, i.e.,

$$V_{\text{Sun}} = \chi V_{\text{shade}}. \tag{15}$$

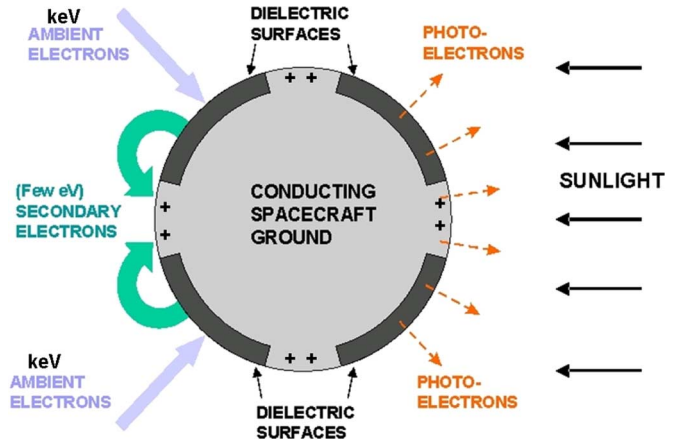


Fig. 3. Schematic scenario of secondary electron suppression by potential wells during spacecraft charging in sunlight. Patches of exposed conducting spacecraft ground among pieces of dielectric surfaces are assumed.

If we neglect conduction currents through the spacecraft from the sunlit to the dark side, a more general multipole expansion is expected to be similar to the limit cases. In such cases, the shaded surfaces charge approximately as in eclipse so that the onset of charging would be relatively unchanged. The multipole models, thus, predict that T^* would be roughly the same in sunlight or eclipse.

In Fig. 2, data are shown of spacecraft potential versus electron temperature [27]. The upper data branch represents charging in eclipse, and the lower data branch is for daylight charging. The lower line (solid) is a fit to the sunlight data, and the upper line (dashed) goes through the eclipse data. The ratio of the two lines is 0.3, which is in rough agreement with the monopole–dipole model at charging threshold. Qualitatively, the onset of charging is the same for sunlight and eclipse.

In the monopole–dipole and monopole–quadrupole models, we have tacitly assumed that the spacecraft surface is uniformly covered with dielectric and the potential distribution is azimuthally symmetric. If this is not true, there could be areas with exposed surface patches at positive potential relative to the dielectrics, producing potential wells and trapping emerging electrons. For example, if the dark side surfaces are mostly covered with dielectric but there are isolated surface elements that are connected electrically to the sunlit side so that they are at a relatively positive potential, escaping secondary electrons would be trapped (Fig. 3). In this way, the secondary emission could be substantially reduced, leading to a lower critical temperature. For this more complicated scenario, there would be differences in the charging onset in sunlight or eclipse because the dark side is no longer isolated from the Sun. Electrical connections between the dark and the sunlit sides by means of grounds or surface/bulk conductivity would also tend to lower the potentials from those in the dipole or quadrupole models, which represent idealized cases. In a complex scenario such as this, there could be trapped photoelectrons on the sunlit side and suppression of secondary electrons on all sides that have barrier formation. Treating the problem fully (with local dielectric hot spots, potential barriers, and wells) would lead to complicated potential distributions without azimuthal

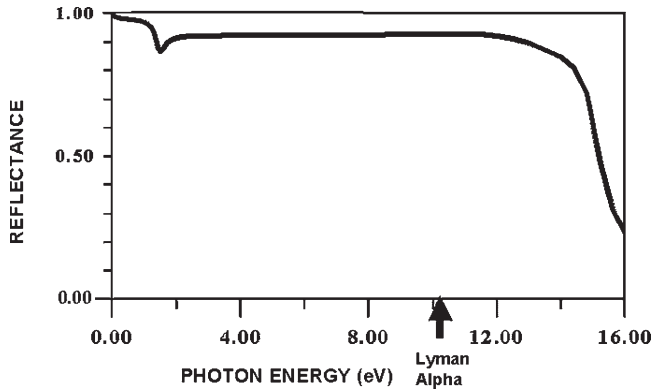


Fig. 4. Reflectance of aluminum at normal incidence. [28], [40].

asymmetry. This problem could be handled, in principle, by the general multipole solution.

V. SURFACE REFLECTANCE

In the spacecraft charging problem, it is important to associate a photoemissivity value to a surface material with regard to the surface condition, surface reflectance, and sunlight intensity. The photoelectron flux $J_{ph}(\omega, \alpha)$ emitted from a surface is given by [36], [37]

$$J_{ph}(\omega, \alpha) = J_o(\omega)Y(\omega, \alpha)[1 - R(\omega, \alpha)] \quad (16)$$

where $J_o(\omega)$ is the incident light intensity at frequency ω , $Y(\omega, \alpha)$ is the photoelectron yield per absorbed photon, α is the photon incidence angle, and R is the reflectance. We remark that the yield [37] can be expressed in terms of photoelectrons emitted per photon absorbed, i.e., $Y = J_{ph}/[J_o(1 - R)]$, or as photoelectrons per incident photon, without the $(1 - R)$ factor in the denominator. Reflectance is a surface property that depends not only on the frequency but also on the material, the smoothness, and the incidence angle [38]. For example, the reflectance R at normal incidence of smooth pure aluminum [39], [40] is about 0.9 at the Lyman Alpha ($Ly\alpha$) frequency of sunlight (Fig. 4), and with protective coating, aluminum mirrors can achieve almost this level of reflectance in space [41]. Highly reflective flat surfaces have been used for concentrating sunlight onto solar cells on satellites such as Telesat Anik F1 and Anik F2 as well as PanAmSat's Galaxy 11 [<http://sat-index.com/failures/702arrays.html>].

Consider a photon beam impacting the surface of a solid. We divide the incident photon flux J_o into two fractions, namely 1) the flux of photons that are reflected, i.e., $J_o R$, and 2) those that penetrate the solid, i.e., $J_o(1 - R)$. Reflected light has almost the same energy as incident light, and little or no energy is imparted at the surface. It is the penetrating photons that impart energy to the material and produce photoelectrons. The solar Lyman Alpha line is about 10 eV in energy, whereas a typical spacecraft surface material has a work function of about 4–5 eV. If an excited electron is created in the solid with sufficient energy, its direction must be such that it can propagate through the material and overcome the work function barrier at the surface. Photoelectrons that emerge from the surface typically have low kinetic energies in the range of 1–3 eV.

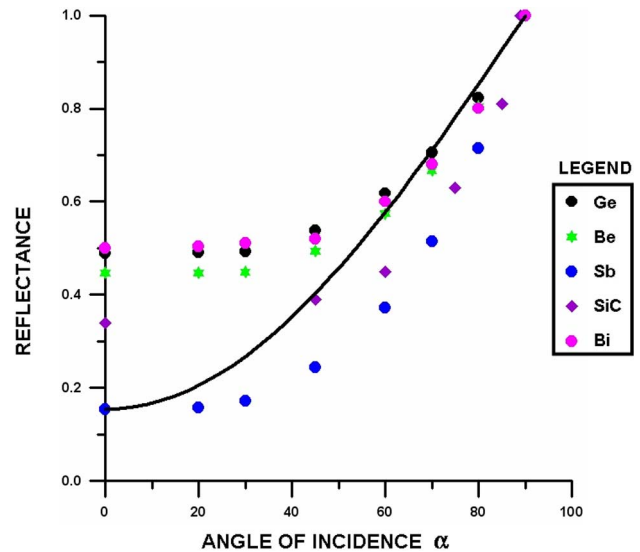


Fig. 5. Reflectance of beryllium, germanium, antimony, Bi, and silicon carbide at various incidence angles. A fit line for Bi is shown (plotted using data taken from [38] and [42]).

The photoelectron yield per absorbed photon Y depends on the interactions mentioned earlier in the setting of the interior (band) structure of the solid. Since the attenuation lengths for incoming photons are functions of photon frequency, the yield can depend strongly on the energy of the incident photon. This photoemission production behavior is described by (16).

It has been conjectured [28] that highly reflective surfaces charge to negative potentials in hot plasmas not only in eclipse but also in sunlight. This is because the photoemission from a highly reflective surface is so low that it is, to some extent, in eclipse conditions. With the large photoemission term greatly reduced, current balance can be obtained during hot plasma events or magnetospheric substorms in the same way as in eclipse.

If this conjecture is confirmed, it may provide an explanation of some reported satellite failures. Mirrors and ordinary surfaces in space will charge to different voltages in sunlight, resulting in differential charging to high voltages, which is a space hazard because it may lead to discharges between surfaces and/or instruments.

VI. COMPETITION WITH AMBIENT ELECTRON CURRENT

We show in Fig. 5 the reflectance as a function of photon angle of incidence for a number of materials. Data have been extracted from published figures [38], [42]. We can make a rough fit to these data in the following form:

$$R(\omega, \alpha) = 1 + (R_o - 1) \cos \alpha \quad (17)$$

where $R_o = R(\omega, 0)$ is the reflectance at normal incidence, and $R(\omega, 90^\circ)$ is unity at grazing. Even if the normal reflectance $R_o = 0$, the reflectance $R(\omega, \alpha)$ at a finite angle α is finite. Equation (17) is fairly typical for a number of materials [38]. A fit line for bismuth (Bi) is shown in Fig. 5. This fit has not been optimized. It gives the correct values at the angles' end points and shows the approximate $\cos \alpha$ behavior, which is all that is

needed for the estimate of the photoemission angle dependence later in this paper.

We now consider the fluxes at a spacecraft surface with the face normal at a given angle α with respect to the Sun's direction. It is assumed that the surface is in a substorm environment and that the main current contributions come from an incoming flux of high-energy electrons along with the outgoing flux of photoelectrons. If $\alpha = 0$, the ratio of the photoelectron flux to that of the ambient electrons at geosynchronous altitudes during a substorm can be taken as

$$\frac{J_{\text{ph}}}{J_e} \approx \frac{2 \text{ nA/cm}^2}{0.5 \text{ nA/cm}^2} \approx 4. \quad (18)$$

Here, J_{ph} is an average photoemission rate for normally incident sunlight [17], and J_e corresponds to a worst case plasma given in [43]. If $\alpha \neq 0$, then the photoelectric current, including reflection, at the relevant frequency, is given by

$$I_{\text{ph}} = \mathbf{J}_o \cdot d\mathbf{A} Y(1 - R) \quad (19)$$

$$\approx J_o dA \cos \alpha \frac{Y_n}{\cos \alpha} (1 - R_o) \cos \alpha \quad (20)$$

$$= J_{\text{ph}} dA (1 - R_o) \cos \alpha \quad (21)$$

where $J_{\text{ph}} = J_o Y_n$. Equation (19) is the basic expression describing photoemission. We show explicitly in (20) the possible $\cos \alpha$ dependence for the terms in (19), and (21) gives the resulting expression. In (19), the first term $\mathbf{J}_o \cdot d\mathbf{A}$ relates to the area perpendicular to the solar radiation and is straightforward. In the third term, i.e., $(1 - R)$, the reflectivity R is represented by the rough fit given in (17). The second term Y is more complex. The behavior of the yield, i.e., $Y = Y_n / (\cos \alpha)$, where Y_n is the yield for normal incidence, is an approximation that depends on the incidence angle and the absorption lengths for a photon L_{ph} and excited electron L_e , in the material [44]. The absorption length for production of an excited electron in the material is on the order of 100\AA but depends markedly on the details of the material band structure. For conductors, the inelastic mean free path of electrons with energies of 10–100 eV is perhaps 5\AA – 10\AA but increases at both higher and lower energies [48]. For insulators, the inelastic mean free path can increase substantially. This approximation breaks down when $L_e / (L_{\text{ph}} \cos \alpha) > 1$. The point at which this occurs is a complex issue not addressed by this paper. When the approximation is operative, the second term cancels one other factor of $\cos \alpha$ so that there is only a single multiplier remaining. It is noted that the spacecraft charging simulation program NASCAP [49] uses a photocurrent of the form $I_{\text{ph}} = s J_{\text{AU}} dA \cos \alpha$, where J_{AU} (user input) is the photoemission rate for an exposed surface area at an ‘‘Earth distance’’ from the Sun, and s (user input) is the ratio of Sun intensity at the spacecraft over the 1-AU value. This formula assumes that the photoemission rate is, on the average, independent of α .

In this paper, we make the conservative assumption that there is one factor of $\cos \alpha$, as indicated in (21). Thus, if a surface is

inclined at an angle α to sunlight and reflection is included, the photoelectron/electron current ratio would be given by

$$P = \frac{I_{\text{ph}}}{I_e} = \frac{J_{\text{ph}}}{J_e} [1 - R_o] \cos \alpha. \quad (22)$$

With smooth pure aluminum surface material, the reflectance R_o at normal incidence is > 0.85 at the $\text{Ly}\alpha$ frequency [39]. At $\alpha = 60^\circ$, using (18) and including reflectance, we get a ratio P of about

$$P = 4(1 - 0.85) \cos 60^\circ \approx 0.3. \quad (23)$$

Here, we have used a conservative value of R_o for smooth aluminum. Modern reflectors in space are very efficient. Advances in optical coatings and materials technology have made possible the development of instruments with substantial improved efficiency for UV space applications. For example, magnesium-fluoride-protected aluminum surfaces have been used on optical components for Hubble Space Telescope instruments, and a reflectance of 0.86 has been achieved [41]. The result for P in (23) has a large uncertainty due to the variability of the geosynchronous environment. However, with this example, we see that the (outgoing) photoelectron current can be less than the (incoming) ambient electron flux at a surface with a combination of high reflectivity and large Sun angle. Therefore, charging to negative voltages can occur in sunlight for such cells, depending on the total net surface currents.

The Mott–Smith–Langmuir orbit-limited model [45], which is often a fairly good approximation for describing current balance at geosynchronous altitudes, is given by

$$I_e(0) [1 - \langle \delta + \eta \rangle] \exp\left(-\frac{q_e V}{kT_e}\right) - I_i(0) \left(1 - \frac{q_i V}{kT_i}\right) = I_{\text{ph}} \quad (24)$$

where the notations are standard (see, e.g., [2]). The term $\langle \delta + \eta \rangle$ describes the effect of secondary and backscatter interactions and is a function of the electron temperature. If we neglect the ion current $I_i(V)$, which is typically much smaller than the electron current at threshold where $V = 0$, the condition for charging is

$$\langle \delta + \eta \rangle = 1 - \frac{I_{\text{ph}}}{I_e(0)} = 1 - P. \quad (25)$$

If P depends on the reflectivity R_o , as in (22), then as R_o increases from 0 to 1, P decreases to 0. When P reaches 0, one recovers the usual condition for determining the critical temperature in eclipse [2].

If the ratio P is greater than 0, the critical temperature will vary. We show in Fig. 6 the value of T^* for three materials, which was calculated versus P . In the calculation, the integrated form of $\langle \delta + \eta \rangle$ as a function T [35], which was derived from published formulas for secondary [46] and backscatter equations [47], was used, and the numerical values for the different materials are the same as given in [33]. The magnitude of the photoemission current was chosen to be less than the ambient electron current ($0 < P < 1$), as could be the case when there is high reflectance. The plot shows that the

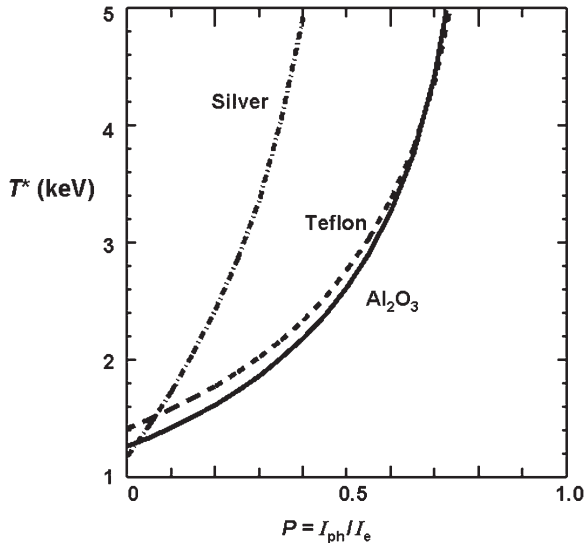


Fig. 6. Effects of photoemission on the critical temperature T^* for the onset of surface charging to negative voltages. The T^* values increase as the ratio P of photoelectron current I_{ph} to the ambient electron current $I_e(V=0)$ increases. At a limiting value of the ratio P for a surface material, the value of T^* is infinity asymptotically. Above this value, charging (to negative voltages) cannot occur.

critical temperature, at which onset of charging occurs, depends strongly on the ratio P , and it increases monotonically with this ratio. As P goes toward 1, there is a limiting value, depending on the material, at which T^* goes to infinity asymptotically. Beyond this value, negative voltage charging cannot occur. The behavior of T^* versus P comes about because increasing P lowers the height of the horizontal line intercepting the $\langle \delta + \eta \rangle$ curve. Since this curve is decreasing, one has to move further out in T_e to find the critical temperature. This situation is illustrated in Fig. 7 for aluminum oxide, and a value of $P = 0.3$. The behavior of the critical temperature is nonlinear due to the nonlinearity of the $\langle \delta + \eta \rangle$ function. As P approaches 1, a solution may not be possible, corresponding to the limiting value for negative sunlight charging by means of direct current balance.

Figs. 6 and 7 describe the general effect. We have assumed unshielded electron current collection and have neglected surface roughness, angular dependence of the secondary and backscatter yields, and ion currents. The value of the critical temperature depends on the validity of the models, and it would improve with increased accuracy of the photoemissivity and surface emission properties.

VII. CONCLUSION

Since the photoemission current exceeds the ambient electron current at geosynchronous altitudes, why do spacecraft charge negatively in sunlight? We have discussed the two mechanisms, namely 1) differential charging and 2) surface reflectance. Differential charging is accompanied by potential barriers that form above photoemitting surfaces, suppressing the escape of photoelectrons and leading to current balance. If differential charging between the sunlit side and the shadowed side occurs, one can model the system as a monopole-dipole.

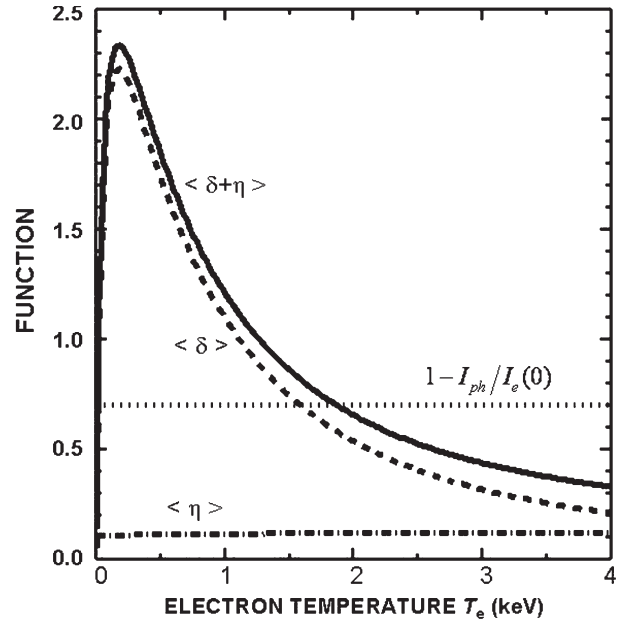


Fig. 7. Shift of the value of critical temperature T^* as a result of photoemission. Without photoemission, T^* is given by the root of $\langle \delta + \eta \rangle = 1$. With photoemission, T^* is given by the root of $\langle \delta + \eta \rangle = 1 - P$.

The monopole-dipole model results show that 1) the ratio of the potential on the sunlit side to that on the shadowed side is approximately 1/3 and 2) the critical temperature T^* is the same as that in eclipse. One can also model the system as a monopole-quadrupole model if the satellite spin is fast and perpendicular to the sunlight direction. The monopole-quadrupole model results show that the ratio becomes approximately 2/5, and by the same argument, the critical temperature T^* is unchanged. A fairly general approximation to the Laplace equation shows that the surface node potentials are linearly related in the same way as for the zero and fast spin limits. In the general multipole configuration, the Sun/shade scaling ratio is unknown, but the behavior of the critical temperature would be similar to the limit cases, except in possible scenarios where there are significant electrical connections between sunlit and dark sides. In these more general scenarios, there may be patches of exposed conductor (relatively positively charged) mixed among areas of dielectric surfaces, such that there is suppression of secondary electron currents and, thus, a modification of the onset of charging. In the second mechanism, we stress the importance of reflectance. Surfaces with higher reflectance generate fewer photoelectrons so that current balance can be achieved without the formation of potential barriers. In magnetospheric substorms, high reflectance surfaces should charge to high negative potentials in hot plasmas, regardless of eclipse or sunlight. We have calculated the critical temperature for several materials in sunlight, using current balance, without invoking differential charging. To show the effect of low photoelectron currents, we vary the ratio of the photoemission to ambient electron current. The exact value of the photoelectron current would depend on the surface condition and, in particular, on the reflectance of the surface material. The results indicate that the value of the critical temperature T^* is shifted, depending on the ratio of the outgoing photoelectron

current to the incoming ambient electron current. Increasing the reflectivity decreases the critical temperature until, in the limit of total reflectance, we recover the eclipse value.

APPENDIX

RELATION BETWEEN THE SURFACE NODE POTENTIALS

The surface nodes are at radius $r = 1$. In rectangular coordinates, the bellyband nodes are located at $+X = (1, 0, 0)$, $-X = (-1, 0, 0)$, $+Y = (0, 1, 0)$, and $-Y = (0, -1, 0)$. Then, we have

$$V(+X) = K (1 + P_1^1(0)A_{11} + P_2^0(0)A_{20} + P_2^2(0)A_{22} + P_3^1(0)A_{31} + P_3^3(0)A_{33}) \quad (\text{A.1})$$

$$V(-X) = K (1 - P_1^1(0)A_{11} + P_2^0(0)A_{20} + P_2^2(0)A_{22} - P_3^1(0)A_{31} - P_3^3(0)A_{33}) \quad (\text{A.2})$$

$$V(+Y) = K (1 + P_1^1(0)B_{11} + P_2^0(0)A_{20} - P_2^2(0)A_{22} + P_3^1(0)B_{31} - P_3^3(0)B_{33}) \quad (\text{A.3})$$

$$V(-Y) = K (1 - P_1^1(0)B_{11} + P_2^0(0)A_{20} - P_2^2(0)A_{22} - P_3^1(0)B_{31} + P_3^3(0)B_{33}). \quad (\text{A.4})$$

Here, we have used the following property of the Legendre functions:

$$P_n^m(0) = 0, \quad \text{if } n + m = \text{odd}$$

to eliminate many terms. We can further write for the nodes at $+Z = (0, 0, 1)$ and $-Z = (0, 0, -1)$

$$V(+Z) = K (1 + P_1^0(1)A_{10} + P_2^0(1)A_{20} + P_3^0(1)A_{30}) \quad (\text{A.5})$$

$$V(-Z) = K (1 + P_1^0(-1)A_{10} + P_2^0(-1)A_{20} + P_3^0(-1)A_{30}). \quad (\text{A.6})$$

Here, we have used the following Legendre property:

$$P_n^m(\pm 1) = 0, \quad \text{if } m \neq 0$$

to simplify. Adding (A.1)–(A.6), we find

$$\begin{aligned} \sum V &= V(+X) + V(-X) + V(+Y) \\ &\quad + V(-Y) + V(+Z) + V(-Z) \\ &= K \{ 6 + A_{10} [P_1^0(1) + P_1^0(-1)] \\ &\quad + A_{20} [4P_2^0(0) + P_2^0(1) + P_2^0(-1)] \\ &\quad + A_{30} [P_3^0(1) + P_3^0(-1)] \}. \end{aligned} \quad (\text{A.7})$$

Using the Legendre function parity relation defined by

$$P_n^m(-x) = (-1)^{n+m} P_n^m(x)$$

and the values

$$P_2^0(0) = -1/2 \quad P_2^0(1) = 1 \quad P_2^0(-1) = 1$$

in (A.7), we find that the terms in square brackets reduce to 0. We are now left with

$$\sum V = 6K$$

which is the desired equation. To reach this result, we have used only the properties of the associated Legendre function ($n \leq 3$) and have made no assumption about the coefficients K , A_{nm} , and B_{nm} .

ACKNOWLEDGMENT

The authors would like to thank M. F. Thomsen for permission to use the magnetospheric plasma analyzer (MPA) data. The Los Alamos MPA measurements were obtained from the CDAWeb data service at the NASA Goddard Space Flight Center. The authors would also like to thank F. Zimmermann, F. Ruggiero, and J. B. Kortright for providing information regarding the dependence of photoemission on the photon incidence angle. The website of AER/Radex, Inc. is <http://www.aer.com/>.

REFERENCES

- [1] J. B. Reagan, R. E. Meyerott, R. W. Nightingale, P. C. Filbert, and W. L. Imhoff, "Spacecraft charging currents and their effects on space systems," *IEEE Trans. Electr. Insul.*, vol. EI-18, no. 2, pp. 354–365, 1983.
- [2] S. T. Lai and D. Della-Rose, "Spacecraft charging at geosynchronous altitudes: New evidence of the existence of critical temperature," *J. Spacecr. Rockets*, vol. 38, no. 6, pp. 922–928, 2001.
- [3] E. C. Whipple, "Potentials of surfaces in space," *Rep. Prog. Phys.*, vol. 44, no. 11, pp. 1197–1250, Nov. 1981.
- [4] D. Hastings and H. B. Garrett, *Spacecraft–Environment Interactions*. Cambridge, UK: Cambridge Univ. Press, 1996.
- [5] B. Feurenbacher and B. Fitton, "Experimental investigation of photoemission from satellite surface materials," *J. Appl. Phys.*, vol. 43, no. 4, pp. 1563–1572, 1972.
- [6] R. Grand, "Properties of the satellite photoelectron sheath derived from photoemission laboratory measurements," *J. Geophys. Res.*, vol. 78, no. 16, p. 2883, 1973.
- [7] H. E. Hinteregger, K. R. Damon, and L. A. Hall, "Analysis of photoelectrons from solar extreme ultraviolet," *J. Geophys. Res.*, vol. 64, no. 8, pp. 961–964, 1959.
- [8] P. R. Stannard *et al.*, *Analysis of the Charging of the SCATHA (P78-20) Satellite*, NASA CR-165348, 1981.
- [9] P. J. Kellogg, "Measurements of potential of a cylindrical monopole antenna on a rotating spacecraft," *J. Geophys. Res.*, vol. 85, no. A10, p. 5157, 1980.
- [10] M. D. Montgomery, J. R. Astridge, S. J. Bame, and E. W. Hones, "Low energy measurements and spacecraft potential: Vela 5 and Vela 6," in *Photons and Particle Interactions With Surfaces in Space*, R. J. L. Grand, Ed. Hingham, MA: Reidel, 1973.
- [11] S. T. Lai, H. A. Cohen, T. L. Aggson, and W. J. McNeil, "Charging of booms on a satellite rotating in sunlight," *J. Geophys. Res.*, vol. 91, no. A11, pp. 12137–12141, 1986.
- [12] A. Pedersen, "Solar wind and magnetospheric plasma diagnostics by spacecraft electrostatic potential measurements," *Ann. Geophys.*, vol. 13, no. 2, pp. 118–129, 1995.
- [13] E. G. Mullen, M. S. Gussenhoven, D. A. Hardy, T. L. Aggson, B. G. Ledley, and E. Whipple, "SCATHA survey of high-level spacecraft charging in sunlight," *J. Geophys. Res.*, vol. 91, no. A2, pp. 1474–1490, 1986.
- [14] S. T. Lai, "High-level spacecraft charging at geosynchronous altitudes: A statistical study," in *Proc. 8th Spacecraft Charging Technology Conf.*, 2003. NASA/CP-2004-213091.
- [15] S. T. Lai and M. Tautz, "High-level spacecraft charging in eclipse at geosynchronous altitudes: A statistical study," *J. Geophys. Res.*, vol. 111, no. A9, p. A09201, doi:10.1029/2004JA010733, 2005.

- [16] U. Fahlson, "Plasma-vehicle interactions in space—Some aspects on present knowledge and future development," in *Photons and Particle Interactions With Surfaces in Space*, R. J. L. Grard, Ed. Dordrecht, Holland: Reidel, 1972.
- [17] M. Mandell, I. Katz, G. Schnuelle, P. Steen, and J. Roche, "The decrease in effective photo-currents due to saddle points in electrostatic potentials near differentially charged spacecraft," *IEEE Trans. Nucl. Sci.*, vol. NS-26, no. 6, pp. 1313–1317, Dec. 1978.
- [18] R. C. Olsen, "Differential and active charging results from the ATS spacecraft," Ph.D. dissertation, Univ. California, San Diego, CA, 1980.
- [19] R. C. Olsen, C. E. McElwain, and E. C. Whipple, "Observations of differential charging effects on ATS-6," *J. Geophys. Res.*, vol. 86, no. A8, pp. 6809–6819, 1981.
- [20] R. C. Olsen and E. C. Whipple, "An unusual charging event on ISEE 1," *J. Geophys. Res.*, vol. 93, no. A6, pp. 5568–5578, 1988.
- [21] H. R. Zhao, C. P. Schmidt, K. Escoubet, K. Torkar, and W. Riedler, "Self-consistent determination of the electronic potential barrier due to the photoelectron sheath near a spacecraft," *J. Geophys. Res.*, vol. 101, no. A7, pp. 15653–15659, 1996.
- [22] T. Nakagawa, T. Ishii, K. Tsuruda, H. Hayakawa, and T. Mukai, "Net current density of photoemission emitted from the surface of the GEOTAIL spacecraft," *Earth Planets Space*, vol. 52, no. 1, pp. 283–292, 2000.
- [23] B. Thiebault, A. Hilgers, E. Sasot, H. Laakso, O. Escoubet, V. Genot, and J. Forest, "Potential barrier in the electrostatic sheath around a magnetospheric spacecraft," *J. Geophys. Res.*, vol. 109, no. A12, p. A12207, doi:10.1029/2004JA010398, 2004.
- [24] M. Soop, "Numerical calculations of the perturbation of an electric field around a spacecraft," in *Photons and Particle Interactions With Surfaces in Space*, R. J. L. Grard, Ed. Dordrecht, Holland: Reidel, 1972.
- [25] D. Higgins, "An analytic model of multi-dimensional spacecraft charging fields and potentials," *IEEE Trans. Nucl. Sci.*, vol. NS-26, no. 6, p. 5162, Dec. 1979.
- [26] A. L. Besse and A. G. Rubin, "A simple analysis of spacecraft charging involving blocked photo-electron currents," *J. Geophys. Res.*, vol. 85, no. A5, pp. 2324–2328, May 1980.
- [27] M. Tautz and S. T. Lai, "Analytic models for a rapidly spinning spherical satellite charging in sunlight," *J. Geophys. Res.*, vol. 110, no. A7, p. A07220, doi:10.1029/2004JA010787, 2005.
- [28] S. T. Lai, "Charging of mirrors in space," *J. Geophys. Res.*, vol. 110, no. A1, p. A01204, doi:10.1029/2002JA009447, Jan. 2005.
- [29] M. Schwartz, *Principles of Electrodynamics*. New York: McGraw-Hill, 1972.
- [30] S. T. Lai and M. Tautz, *Spacecraft Charging in Sunlight: New Evidence of Monopole-Dipole Potential Distribution*, 2006. to be submitted for publication.
- [31] S. T. Lai, M. S. Gussenhoven, and H. A. Cohen, "Energy range of ambient electrons responsible for spacecraft charging," *EOS Trans. Amer. Geophys. Union.*, vol. 63, no. 18, p. 421, 1982.
- [32] J. G. Laframboise, R. Godard, and M. Kamitsuma, "Multiple floating potentials, threshold temperature effects, and barrier effects in high voltage charging of exposed surfaces on spacecraft," in *Proc. Int. Symp. Spacecr. Mater. Space Environ.*, Toulouse, France, 1982, pp. 269–275.
- [33] J. G. Laframboise and M. Kamitsuma, "The threshold temperature effect in high voltage spacecraft charging," in *Proc. Air Force Geophys. Workshop Natural Charge. Large Space Struct. Near Earth Polar Orbit*, pp. 293–308. AFRL-TR-83-0046, ADA-134-894, 1983.
- [34] S. T. Lai, M. S. Gussenhoven, and H. A. Cohen, "The concepts of critical temperature and energy cutoff of ambient electrons in high voltage charging of spacecraft," in *Proc. 17th ESLAB Symp.*, D. Guyenne and J. H. A. Pedersen, Eds, Noordwijk, The Netherlands, 1983, pp. 169–175.
- [35] S. T. Lai, "Spacecraft charging thresholds in single and double Maxwellian space environments," *IEEE Trans. Nucl. Sci.*, vol. 38, no. 6, pp. 1629–1634, Dec. 1991.
- [36] J. A. R. Samson, *Techniques of Ultraviolet Spectroscopy*. New York: Wiley, 1967.
- [37] W. E. Spicer, "Photoelectric emission," in *Optical Properties of Solids*, F. Abelés, Ed. Amsterdam, The Netherlands: North Holland, 1972, pp. 755–858.
- [38] C. J. Powell, "Analysis of optical and inelastic electron scattering data—III: Reflectance data for beryllium, germanium, antimony, and bismuth," *J. Opt. Soc. Amer.*, vol. 60, no. 2, pp. 214–220, 1970.
- [39] J. G. Endriz and W. E. Spicer, "Study of aluminum films—I: Optical studies of reflectance drops and surface oscillations on controlled-roughness films," *Phys. Rev. B, Condens. Matter*, vol. 4, no. 12, pp. 4144–4150, 1971.
- [40] *CRC Handbook of Chemistry and Physics*, 82nd ed. D. R. Lide, Ed. Boca Raton, FL: CRC Press, 2002.
- [41] R. A. M. Keski-Kuha, J. I. Larraquert, J. S. Gum, and C. M. Fleetwood, "Optical coatings and materials for ultraviolet space applications," in *Proc. Ultraviolet-Opt. Space Astron. Beyond HST*, Astron. Soc. Pac. Conf. Ser., 1999, vol. 164, pp. 406–408.
- [42] J. B. Kortright and D. L. Windt, "Amorphous silicon carbide coatings for extreme ultraviolet optics," *Appl. Opt.*, vol. 27, no. 14, pp. 2841–2846, 1988.
- [43] C. Purvis, H. B. Garrett, A. C. Whittlesey, and N. J. Stevens, *Design Guidelines for Assessing and Controlling Spacecraft Charging Effects*, NASA Tech. Paper 2361, 1984.
- [44] J. B. Jeanneret, *Photoemission at LHC—A Simple Model*, CERN/Note 97-48 (AP), 1997.
- [45] H. Mott-Smith and I. Langmuir, "The theory of collectors in gaseous discharges," *Phys. Rev.*, vol. 28, no. 4, pp. 727–763, Oct. 1926.
- [46] N. L. Sanders and G. T. Inouye, "Secondary emission effects on spacecraft charging: Energy distribution consideration," *Spacecraft Charging Technology*, NASA-2071, ADA-08426, AFRL, 1978.
- [47] S. M. Prokopenko and J. G. L. Laframboise, "High voltage differential charging of a geostationary spacecraft," *J. Geophys. Res.*, vol. 85, no. A8, pp. 4125–4131, Aug. 1980.
- [48] C. J. Powell and A. Jablonski, *Electron Inelastic Mean Free Path Database*. Gaithersburg, MD: Nat. Inst. Standards Technol., 2000.
- [49] M. J. Mandell, V. A. Davis, and I. T. Mikellides, "NASCAP-2K user's manual," Sci. Appl. Int. Corp., San Diego, CA, SAIC Rep. 02/2047, Version 1.1, May 2003.



Shu T. Lai (M'80–SM'88–F'05) received the Ph.D. degree in physics from Brandeis University, Waltham, MA, in 1971, and the Certificate of Special Studies in Administration and Management from Harvard University, Cambridge, MA, in 1986.

He is a Senior Physicist with the Space Weather Center of Excellence, Space Vehicles Directorate, Air Force Research Laboratory, Hanscom Air Force Base, Bedford, MA. He was previously with the Lincoln Laboratory, Massachusetts Institute of Technology, Cambridge. He has more than 80 publications, including papers in areas of spacecraft surface charging, deep dielectric charging, mitigation techniques, critical velocity ionization in the vicinity of spacecraft, and hypervelocity impacts on spacecraft. He is also the holder of three patents.

Dr. Lai is a Fellow of the Institute of Physics, a Fellow of the Royal Astronomical Society, and an Associate Fellow of the American Institute of Aeronautics and Astronautics (AIAA). He was a Guest Editor of the IEEE TRANSACTIONS ON PLASMA SCIENCE, Special Issue on Space Plasmas, in December 2000. He was the Chair of the IEEE Nuclear and Plasma Sciences Chapter, IEEE New England Section, during 1993–1996. He has chaired numerous sessions in conferences of the IEEE, AIAA, American Geophysical Union (AGU), and American Physical Society (APS), as well as in spacecraft charging technology conferences. He also served as the Chair of the AIAA Atmospheric and Space Environments Standards Committee during 1996–2002 and the Chair of the AIAA Atmospheric and Space Environments Technical Committee from January 2003 to January 2005.



Maurice F. Tautz (M'04) was born in Victoria, BC, Canada, on October 29, 1941. He received the B.Sc. and M.S. degrees from the University of Victoria, Victoria, BC, in 1964 and 1968, respectively, and the Ph.D. degree in elementary particle physics from the Northeastern University, Boston, MA, in 1976.

He is with Atmospheric and Environmental Research (AER)/Radex, Lexington, MA, and is currently working onsite at the Air Force Research Laboratory, Hanscom Air Force Base, Bedford, MA. His main research interest is in computer simulations

and analytical modeling of spacecraft charging problems.